Korea-Australia Rheology Journal
Vol. 12, No. 1, March 2000 pp. 83-92

Optimization of filling process in RTM using genetic algorithm

Byoung Yoon Kim, Gi Joon Nam, Ho Sok Ryu and Jae Wook Lee*
Department of Chemical Engineering, Sogang University
[1]Shinsu-Dong, Mapo-Ku, Seoul, 121-742, Korea
(Received February 2, 2000)

Abstract

In resin transfer molding (RTM) process, preplaced fiber mat is set up in a mold and thermoset resin is injected into the mold. An important interest in RTM process is to minimize cycle time without sacrificing part quality or increasing cost. In this study, the numerical simulation and optimization process in filling stage were conducted in order to determine the optimum gate locations. Control volume finite element method (CVFEM) was used in this numerical analysis with the coordinate transformation method to analyze the complex 3-dimensional structure. Experiments were performed to monitor the flow front to validate simulation results. The results of numerical simulation predicted well the experimental results with every single, simultaneous and sequential injection procedure. We performed the optimization analysis for the sequential injection procedure to minimize fill time. The complex geometry of an automobile bumper core was chosen. Genetic algorithm was used in order to determine the optimum gate locations with regard to 3-step sequential injection case. These results could provide the information of the optimum gate locations in each injection step and could predict fill time and flow front.

Keywords: resin transfer molding, control volume finite element method, coordinate transformation, genetic algorithm, process optimization

1. Introduction

Liquid composite molding (LCM) processes are versatile and efficient means for producing fiber-reinforced plastic composite structures. In a typical LCM cycle, thermoset resin is injected into a mold filled with preplaced fiber reinforcement. The resin wets out the fiber until the mold is filled, and then cured, generally via the addition of heat. LCM processes are divided into two categories, resin transfer molding (RTM) and structural reaction injection molding (SRIM). In RTM, resin is injected slowly and little heat transfer nor chemical reaction take place until the mold is filled. Thus the entire cycle can be viewed as two separate stages, i.e. fill and cure. Fill times in RTM range from a few minutes to several hours. Typical fill times in SRIM are less than 1 min and an entire cycle from fill to demolding is completed about 5~10 minutes. This study concentrates on the numerical and experimental analysis of the flow issues associated with RTM.

Because mold cost increases with part complexity, numerical simulation of RTM process is becoming more and more important. A simulation for filling stage in RTM will reduce the time required to design a mold and also assure the quality of the products. Several researchers have published dealing with the numerical modeling. Bruschke and Advani (1990) developed a 2-dimensional numerical scheme, and Young and *et al.* (1991) developed 2 and 3-dimensional schemes by control volume finite element method (CVFEM) for the filling stage. Chan and Hwang (1988) developed 2-dimesional numerical model by least squares FEM, Wu and Hourng (1995) simulated filling process in order to explain the phenomena of edge effects by the boundary fitted FEM, and Yoo (1996) developed 2-dimensional model by the boundary element method. Phelan Jr. (1997) simulated filling process using 2 and 3-dimensional FEM and flow analysis network (FAN).

An important interest in RTM process is to minimize cycle time without sacrificing part quality and increasing cost. There are a lot of processing variables in RTM process, and one of the most critical factors is to determine gate location, which is especially important in complex mold geometry. Determining gate locations by trial and error is not practical because the retooling is expensive and time inefficient, which was mentioned in prior work by Pandelidis and Zou (1990), Noller (1991) and Catoen (1993). A numerical simulation to predict these variables can provide a design tool, once the locations of inlet gates has been specified. There are so many possible choices for gate locations as node numbers in the finite element mesh for the mold geometry, however. In addition to that, the fill

*Corresponding author: jwlee@ccs.sogang.ac.kr

time with respect to the location of gates is nonlinear, hence there is a necessary for developing systematic search method which can be interactively coupled with filling simulation capabilities to determine optimum gate locations. We used the genetic algorithm (GA) as a searching method, which was proposed by Goldberg (1989), in this study. GA was applied to search method by Caroll (1996) for dealing with highly nonlinear and large spaces having many possible local optima. An optimization study of finding gate and vent locations using GA was performed by Mathur and *et al.* (1999) in case of simple 2-dimensional geometry.

Another important variable in process design is the injection pressure. The injection pressure directly affects the industrial costs. The use of multiple port injection can greatly speed up mold filling for large part without increasing injection pressure. Though the simultaneous multiple injection process can dramatically reduce fill time, the process has the potential of containing much void contents where two or more flow fronts meet. The sequential injection process, proposed by Chan (1992), was used in this study to minimize cycle time without sacrificing part quality and increasing cost.

2. Theory

2.1. Control Volume Finite Element Method

In order to simulate the filling process, several assumptions must be made to simplify the problem. In the present study, the preplaced fiber mat in mold cavity are assumed rigid, and no deformation during mold filling. Inertia effects are neglected because of low Reynolds number of the resin flow. Furthermore, surface tension is considered negligible, as compared with the dominant viscous force.

The mold cavity is assumed to be much larger than the pore size of the fiber mat. Therefore, Darcys law flow through porous media can be used to replace the momentum equation. It can be written as following

$$\vec{v} = -\frac{\bar{\bar{k}}}{\mu} \cdot \nabla P \tag{1}$$

where $\vec{v}$ is velocity vector, $\bar{\bar{k}}$ is permeability tensor, μ is viscosity, and ∇P is pressure gradient. In a 3-dimensional flow field under Cartesian coordinates, the velocity vector consists of three components, u, v and w, in the x, y and z directions, respectively. Eq.1 can then be written as

$$\begin{bmatrix} u \\ v \\ w \end{bmatrix} = -\frac{1}{\mu}\begin{bmatrix} k_{xx} & k_{xy} & k_{xz} \\ k_{yx} & k_{yy} & k_{yz} \\ k_{zx} & k_{zy} & k_{zz} \end{bmatrix}\begin{bmatrix} \frac{\partial P}{\partial x} \\ \frac{\partial P}{\partial y} \\ \frac{\partial P}{\partial z} \end{bmatrix} \tag{2}$$

where k_{ij} ($i,j = x, y$ and z) are the components of the permeability tensor. For an incompressible fluid, the continuity equation can be reduced as

$$\frac{\partial u}{\partial x} + \frac{\partial v}{\partial y} + \frac{\partial w}{\partial z} = 0 \tag{3}$$

In many RTM applications, the mold geometry is often considered to be 2-dimensional, which means that the dimension of thickness is much smaller than those of the planar directions. Therefore, mold filling in a thin cavity can be modeled as a 2-dimensional flow. The local coordinates are chosen in such a way that z axis is always along the thickness direction. Thus, the formulation is based on a local system, and the geometry data is mapped into this local coordinate system along the part surface. Since the pressure gradient in the thickness direction is negligibly small compared with those in other directions, the pressure is assumed to be constant in the z direction. By assuming pressure to be a function of only x and y, Eq. 2 can be written in a 2-dimensional form.

$$\begin{bmatrix} u(x,y,z) \\ v(x,y,z) \end{bmatrix} = -\frac{1}{\mu(x,y,z)}\begin{bmatrix} k_{xx} & k_{xy} \\ k_{yx} & k_{yy} \end{bmatrix}\begin{bmatrix} \frac{\partial P(x,y)}{\partial x} \\ \frac{\partial P(x,y)}{\partial y} \end{bmatrix} \tag{4}$$

In order to eliminate the independent variable z in the above equation, the velocity is averaged through z direction, i.e.

$$\begin{bmatrix} \bar{u}(x,y) \\ \bar{v}(x,y) \end{bmatrix} = \frac{1}{h_z}\int_{-h_z/2}^{h_z/2}\begin{bmatrix} u(x,y,z) \\ v(x,y,z) \end{bmatrix} dz = -\begin{bmatrix} s_{xx} & s_{xy} \\ s_{yx} & s_{yy} \end{bmatrix}\begin{bmatrix} \frac{\partial P(x,y)}{\partial x} \\ \frac{\partial P(x,y)}{\partial y} \end{bmatrix} \tag{5}$$

and

$$\begin{bmatrix} s_{xx} & s_{xy} \\ s_{yx} & s_{yy} \end{bmatrix} = \frac{1}{h_z}\int_{-h_z/2}^{h_z/2}\frac{1}{\mu(x,y,z)}\begin{bmatrix} k_{xx} & k_{xy} \\ k_{yx} & k_{yy} \end{bmatrix} dz \tag{6}$$

where h_z is part thickness and the s_{ij} is flow coefficient with average values of viscosity and permeability in the thickness direction. The boundary conditions of Eq. 5 in the local coordinate system are following.

$$\left.\frac{\partial p}{\partial n}\right|_{wall} = 0,\ p|_{front} = 0,\ p|_{gate} = p_0 \text{ or } \bar{v}|_{gate} = \bar{v}_0 \tag{7}$$

The part thickness, h_z, in Eq. 6 may vary from one element to another within a finite element model. By using divergence theorem, Eq. 5 with Eq. 3 can be written as

$$\int_C h_z \begin{bmatrix} n_x & n_y \end{bmatrix}\begin{bmatrix} s_{xx} & s_{xy} \\ s_{yx} & s_{yy} \end{bmatrix}\begin{bmatrix} \frac{\partial P}{\partial x} \\ \frac{\partial P}{\partial y} \end{bmatrix} dL = 0 \tag{8}$$

The entire flow field is constructed by a number of three-node triangular elements. Each element is divided into three sub-areas by the lines connecting the centroid of the

element to the midpoint of each side. A control volume is composed of several sub-areas, which have a common node at the center of the control volume.

The mold filling can be regarded as a quasi-steady state process by assuming a steady state condition at each time step. This can be solved by considering the transient solution to be a sequence of steady-state solutions separated by many small time increments. Boundaries of a flow domain in the mold filling include the mold walls, inlets and flow front. There is no flow in the direction normal to the mold wall, the first derivative of pressure normal to the wall is zero. In case of specified injecting flow rate, a specified flow rate is assigned to the control volumes including the injecting nodes. For the case of specified injecting pressure, a specified pressure can be assigned to the inlet nodes.

A parameter F is used to represent the status of each control volume of the flow domain at the flow front. If the control volume is partially filled, F is equal to the volume fraction of the fluid occupying the control volume. The control volumes with F values between 0 and 1 are considered as flow front elements. The node pressures in the partially filled flow front control volumes are set to zero. With the above-described boundary conditions, the set of linear algebraic equations developed in 2-dimensional formulation can be solved to determine the pressure field during mold filling.

The simulation program assumes that the control volumes enclosing the inlet nodes are filled with fluid at the beginning of mold filling. After pressure field is determined, the velocity can be evaluated according to Darcys law. For a selected time increment, the volume of resin into each flow front control volume (0<F<1) is calculated on the basis of the velocity field. The calculated volume of resin inflow is added to the original flow front control volume. If the total resin volume in a control volume is equal to the volume of the control volume, that control volume is considered "full" (F = 1). The time increment is selected in such a way that one control volume will be filled in each time step. Sometimes, several control volumes can be filled simultaneously. The restriction the time increment ensures the stability of the quasi-steady state approximation. The new flow front in each time step can be estimated according to the velocity vector in the flow front and the time increment after the pressure field is determined. After the value F is updated, another pressure computation is performed for all the control volumes with F = 1. The procedure is repeated until the whole mold cavity is filled. The time for a control volume to be half filled is assumed to be the exact time when the flow front reaches the node within the control volume. In this way, the time for the flow front to reach each node within the mold cavity can be known. The flow front profile can be determined by interpolating and connecting the positions with the same fill time.

2.2. Permeability Characteristics

Darcys law relates the fluid flow to the pressure gradient using the fluid viscosity and the permeability of the porous medium. The permeability can be characterized as a function of the porous medium structure and porosity. The porosity can be written as

$$\phi = 1 - \frac{n\xi}{t\rho_f} \tag{9}$$

where n is the number of the fiber mat inside the mold, ξ is the surface density, t is the thickness of the mold cavity, and ρ_f is the density of the glass fiber in the reinforcement.

In the isotropic fiber mat, the fluid expands to radial direction before the flow front contacts the side wall. During this period, Darcys law can be rewritten in the cylindrical coordinates as

$$\frac{\partial^2 P}{\partial r^2} + \frac{1}{r}\frac{\partial P}{\partial r} + \frac{1}{r^2}\frac{\partial^2 P}{\partial \theta^2} = 0 \tag{10}$$

A boundary condition imposed at the moving front requires that the boundary propagates with the local fluid velocity. For the radial flow, the differential equation can be obtained as

$$\frac{dR_f}{dt} = \frac{k\Delta P}{\phi\mu}\frac{1}{R_f \ln(R_f/R_o)} \tag{11}$$

where R_o and R_f are the radii at the inlet and flow front and ΔP is the pressure difference between them. Subjected to the initial condition, i.e., $R_f = R_o$ at t = 0, then the solution is calculated as

$$G(\delta_f) = \frac{\delta_f^2(2\ln\delta_f - 1) + 1}{4} = \Phi \tag{12}$$

where $\delta_f (= R_f/R_o)$ is a dimensionless radial extent, $G(\delta_f)$ is the dimensionless penetration length and Φ $(= k\Delta Pt/\phi\mu R_o^2)$ is a dimensionless flow time.

The total pressure(P_t) can be expressed as

$$P_t = P_m + P_g + P_v + P_c \tag{13}$$

where P_m is the applied mechanical pressure, p_g is the gravitational pressure, P_v is the vacuum pressure and P_c is the capillary pressure attributed to surface tension. In this study, the applied mechanical pressure is quite high compared to the gravitational pressure and the vacuum process is not used. Thus Eq. 12 can be rewritten as

$$G(\delta_f) = \frac{kt}{\phi\mu R_\delta^2}(\Delta P_m + \Delta P_c) \tag{14}$$

From Eq. 14 the permeability can be calculated from the slope of the dimensionless penetration length as a function

of applied pressure.

2.3. Genetic Algorithm

The current literature identifies three main types of searching methods. They are classified as calculus-based, enumerative and random by Goldberg (1989). Calculus-based methods are local in scope, because the optima they seek are the best in a neighborhood of current point. This methods also depend on the existence of derivatives, that is well-defined slope values, but the real process of search has discontinuities and vast multi-modal, noisy search spaces as shown in Fig. 1(a). Enumerative schemes look at objective function values at every point in the search space, one at a time. This scheme is discounted in robustness because of its lack of efficiency. Random search algorithms have achieved increasing popularity because of the shortcomings of calculus-based and enumerative schemes. The genetic algorithm in this study is an example of search procedure that used random choice as a tool to guide a highly exploitative search through coding of a parameter space.

A genetic algorithm operates on the Darwinian principle of survival of the fittest. An initial population size n is created from a random selection of parameters in the parameter space. Each parameter set represents the individuals chromosomes. Each of the individuals is assigned a fitness based on how well each individuals chromosomes allow it to perform in its environment. The process of mating and child creation is continued until an entirely new population of size n is generated with the hope that strong parents will create a fitter generation of children; in practice, the average fitness of the population tends to increase with each new generation. The fitness of each of the children is determined and the process if selection, crossover and mutation are repeated. Successive generations are created until very fit individuals are obtained.

There are three operations which occur in GA to create the next generations such as selection, crossover and mutation as shown in Fig. 1(b). Fit individuals are selected for mating, while weak individuals die off. Mated parents create a child with a chromosome set that is some mix of the parents chromosomes. For example, Parent #1 has chromosomes 'abcde', while Parent #2 has chromosomes 'ABCDE' through the selection operator. A possible chromosome set for the child is the 'abcDE, where the position between the 'c' and 'D' chromosomes is the crossover point. This is called single-point crossover because a crossover point is randomly chosen where the chromosome set of the second parent overwrites the chromosome set of the first parent. It is also possible to obtain any combination of two parents chromosomes such as 'aBcDe', as called uniform crossover. There is a small probability that one or more of the childs chromosomes will be mutated, such as jump and creep mutation. The jump mutation produces a chromosome which is randomly picked and mutated, e.g. the child ends up with chromosomes 'abcDK'. In creep mutation, the child ends up with chromosomes 'abcDF', where F was not a chromosome from either parent, but is only one increment away from parent #2s chromosome value of E.

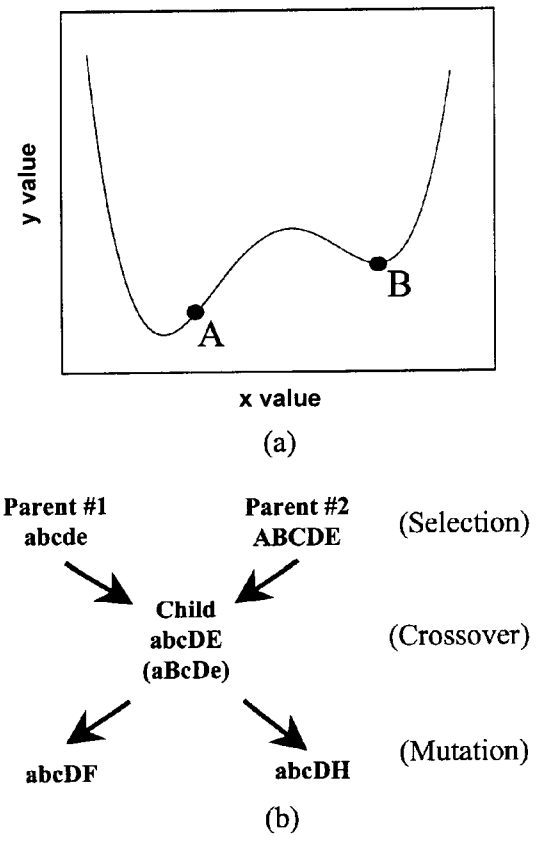

Fig. 1. A brief description of Genetic Algorithm.
A : near global peak by GA and local peak, B : local peak by gradient decrease method three GA operators, i.e. selection, crossover and mutation.

3. Experimental

Experimental apparatus used in this study was illustrated in Fig. 2. A volumetric dispacement pump, a motionless mixer and a control console were used to inject the resin through the fiber mat placed two mold plates. The 400 mm by 210 mm aluminum plates of the mold were designed to 3 and 5 mm thickness with 4 inlet gates, 4 vents, 12 sensors and a 17.5 mm diameter insert. The schematic of the mold used in this study was represented in Fig. 3. In order to monitor the flow front during the filling process, the upper plate was made of acrylate and the video camera was set on the mold. Resin position sensor system developed by Lee and *et al.* (1998) was used to measure the penetration length with time.

Unsaturated polyester (UP) and E-glass fiber were used

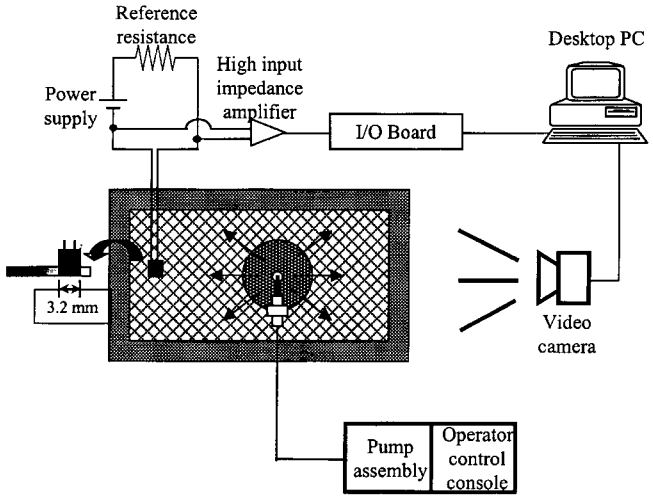

Fig. 2. Schematics of experimental setup for flow front and permeability measurement.

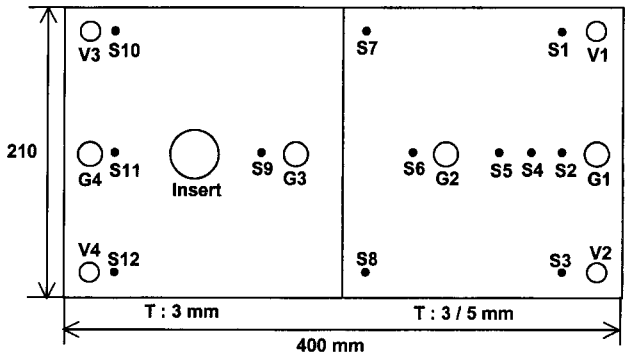

G:gate, V:vent, S:resin position sensor

Fig. 3. Schematic of mold geometry.

as experimental materials in this study. The viscosity change with shear rate of UP at each temperature was measured using a plate and plate geometry in ARES, and it was shown that UP exhibited a behavior of Newtonian fluid. Newtonian flow condition was used in numerical simulation by assuming no cure during the filling stage. The fiber material used in this study was E-glass fiber supplied by Keumgang Chemical Co. Ltd. The physical properties of UP and E-glass fiber used in numerical simulation were listed in Table 1.

Experiments were conducted to confirm the results of the numerical simulation. Good contact between the fiber mat and the walls is necessary to prevent flow channeling, hence a sealant was preplaced around the perimeter of the mold cavity to compress and clamp the edges of the fiber mat. The inlet condition was chosen to constant pressure, which was fixed at 20 *psi*. Throughout all the experiments the photographs were taken during the filling stage in order to measure the flow front positions at each time step.

Table 1. Material properties of E-glass fiber and unsaturated polyester

Material	Properties	Unit	Value
E-glass Fiber	Density	g/cm^3	2.56
	Surface density	g/m^2	450
	Linear coefficient of thermal expansion	$T[K]^{-1}$	5.0×10^{-6}
	Heat capacity	J/kg-K	794.94
	Heat conductivity	W/kg-m	0.89
Unsaturated Polyester	Viscosity(15~80°C)	poise	$1.4\times10^{-5}\times$ exp(3934.56/T[K])
	Density	g/cm^3	1.1
	Linear coefficient of thermal expansion	$T[K]^{-1}$	1.1×10^{-4}
	Heat capacity (20~80°C)	J/kg-K	5450.5+ 37.06×T[K]
	Heat conductivity	W/kg-m	2.434

4. Results and Discussions

4.1. Permeability Measurement

The in-plane permeability of resin in the fiber mat was obtained in the rectangular mold with fiber mats of 7 to 10 layers. The ranges of inlet pressure in these experiments were varied from 20 to 30 *psi*. The effects of applied pressure to the permeability at different porosity was investigated. The permeability was constant through the applied pressure and increased as the porosity increased as shown in Fig. 4. The Kozeny-Carman equation fitted well with the experimental data in Fig. 5 and could be expressed by following relationship.

$$K = 4.581\times10^{-10}\frac{\phi^3}{(1-\phi)^2} \quad (15)$$

4.2. Comparison with Numerical and Experimental Results

In order to confirm the predicted mold filling results obtained from the numerical analysis, comparison of experimental and numerical analysis for rectangular mold were carried out in various cases. All cases and their comparison of fill time were summarized in Table 2.

At first, single injection cases were compared and it was represented in Fig. 6. Fig. 6(a) showed flow pattern in a simple rectangular mold and Fig. 6(b) represented it in a mold that had a round insert. The numerical analysis showed that the flow front was initially circular around the injection port and gradually revealed a shape of straight line. However, the behavior from experiment lagged the numerical movement at mold wall throughout filling proc-

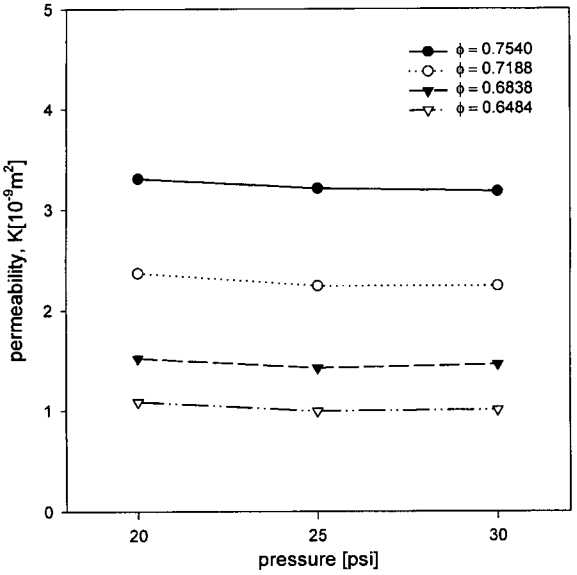

Fig. 4. Permeability vs. applied pressure for various porosity.

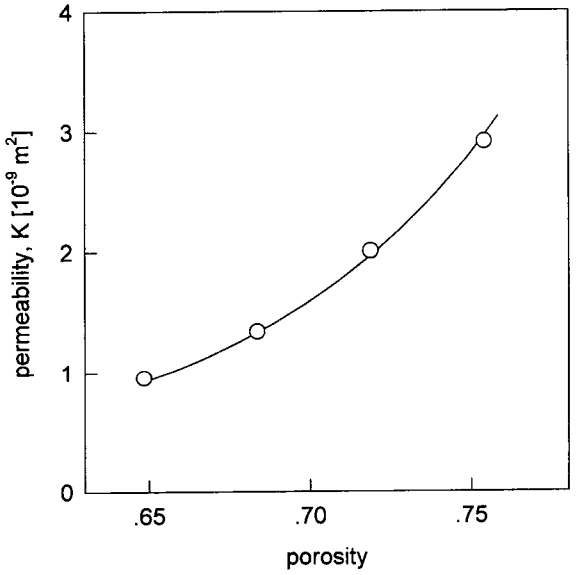

Fig. 5. Permeability vs. porosity(circle) and its curve fits using Kozeny-Carman eqn(line).

ess. This deviation was thought to be related to the installation of sealant at the mold wall. Despite these deviations, the experimental flow fronts and fill times agreed reasonably well with the numerical results. The comparison of case 1 and case 2 in Table 2 showed that the insert had little effect on the filling pattern if it was located far from the gate.

Fig. 7 represented the effect of different permeability on flow patterns. In Fig. 7(a), the gate was located in the mold having the higher permeability and was vice versa in Fig. 7(b). The fill time was reduced when the gate was located in the mold having higher permeability. If there was no insert, the degree of fill time reduction became

Table 2. Processing conditions used in the analysis of rectangular mold cavity

Geometry		Gate	Fill Time [sec]		Case
Insert	Thickness	Location	Numerical	Experiment	No.
No insert	3 mm	1	1065	1020	1
		4→3→2	546	504	7
		2, 3, 4	97	-	8
	3/5 mm	1	575	570	3
		4	624	611	4
		1→2→3	312	292	9
		4→3→2	352	331	10
Insert	3 mm	1	1057	1010	2
	3/5 mm	1	571	562	5
		4	638	623	6
		1→2→3	315	286	11
		4→3→2	366	329	12

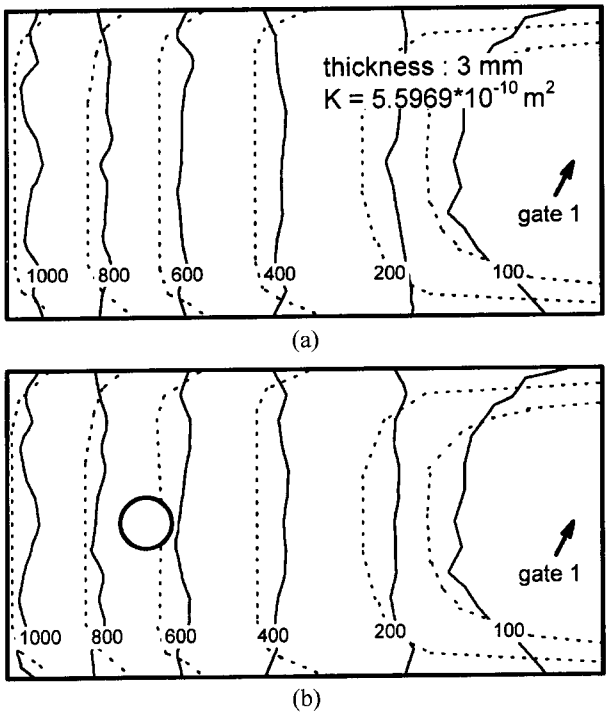

Fig. 6. Experimental(dot) and numerical(solid) flow fronts in the filling of rectangular mold.
(a) case 1 in Table 2 : $t_{fill,exp}$ = 1020 sec, $t_{fill,sim}$ = 1065 sec
(b) case 2 in Table 2 : $t_{fill,exp}$ = 1010 sec, $t_{fill,sim}$ = 1057 sec.

somehow small as shown in case 3 and case 4 in Table 2. From this result the fill time was related not only to the difference of the permeability but also to the distance between the gate and the insert. If the insert was located near in the gate, it acted as the barrier against the filling

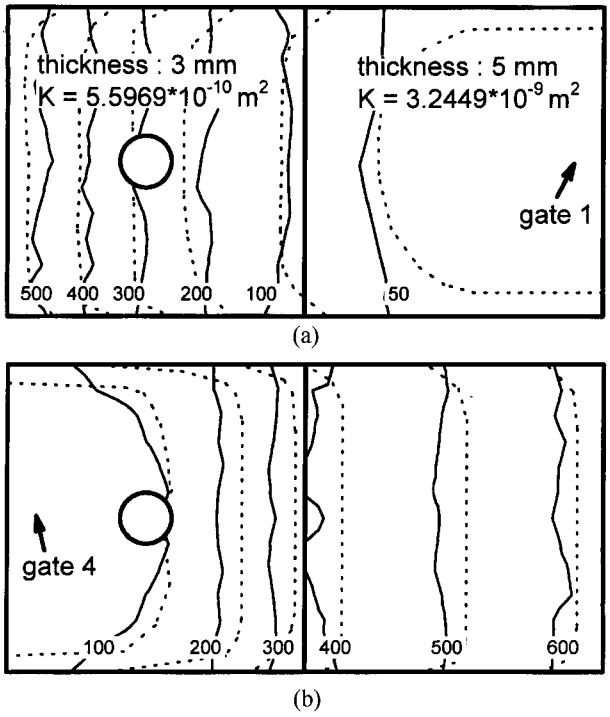

Fig. 7. Experimental(dot) and numerical(solid) flow fronts in the filling of rectangular mold.
(a) case 5 in Table 2 : $t_{fill,exp}$ = 562 sec, $t_{fill,sim}$ = 571 sec
(b) case 6 in Table 2 : $t_{fill,exp}$ = 623 sec, $t_{fill,sim}$ = 638 sec

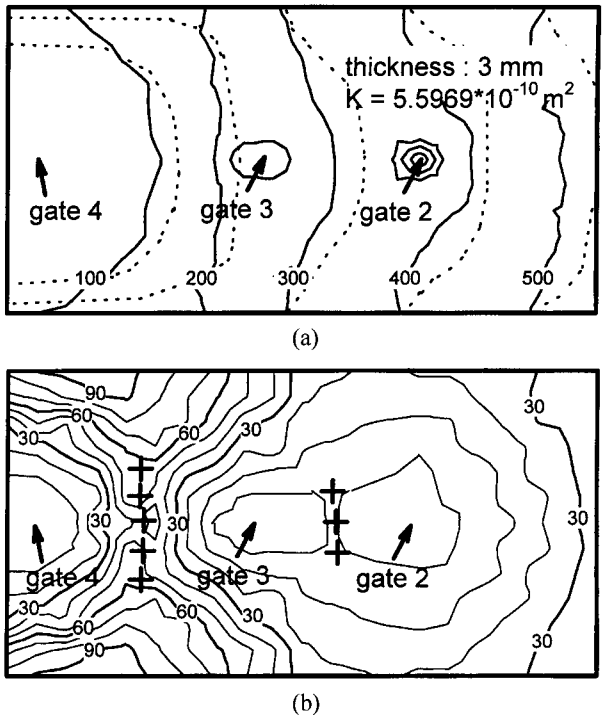

Fig. 8. Experimental(dot) and numerical(solid) flow fronts in the filling of rectangular mold.
(a) case 7 in Table 2 : $t_{fill,exp}$ = 504 sec, $t_{fill,sim}$ = 546 sec
(b) case 8 in Table 2 : $t_{fill,sim}$ = 97 sec (weld line denoted by cross symbol)

process.

The results of the various filling processes were investigated. The comparison between the simultaneous and sequential injection process was shown in Fig. 8(a) and (b). Though the former was much better than the latter from the viewpoint of fill time, the former had two weld lines, i.e. two different flow with the opposite direction met each other. It was marked cross symbol in Fig. 8(b). It may caused the void in cavity and deteriorated the quality of the product. When the sequential injection scheme was used, an enhancement in mold filling rate was achieved without weld line. Fill times in various sequential injection processes(cases 9 to 12) were listed in Table 2. There were fairly good correspondence between experimental and simulation results. The tendency with the location of insert was similar to that of single injection, but the effect of the insert was somehow reduced relatively.

4.3. Filling Process Optimization of 3-Dimensional Complex Structure

An automobile bumper core having complex structure was chosen as a target model to optimize filling process using genetic algorithm, and its picture was represented in Fig. 9(a). In order to apply this structure to CVFEM, the finite element mesh was generated having 590 nodes and 940 elements as shown in Fig. 9(b). Because of symmetry, only the half geometry having 299 nodes and 470 elements was used in this numerical study. Since general injection pressure used in RTM industry was often less than 100 *psi*, the inlet pressure was set to 60 *psi* in this study.

At first, a number of case studies were intuitively performed for various processing conditions to find the optimum gate location and their results were summarized in Table 3. These cases were divided into three types according to injection methods, which were simultaneous, 2-step sequential and 3-step sequential injection, respectively. Four case studies with different gate locations were performed in simultaneous injection. Although the gate location having minimum fill time was found out to be the case 3, weld line was generated. Therefore the optimum gate location was determined to be the case 4 for simultaneous injection process. In case of 2-step sequential injection, the gate location having minimum fill time was turned out to be the case 8 and its flow pattern was represented in Fig. 10(a). In case of 3-step sequential injection, the optimum gate location was determined to be the case 10 as shown in Fig. 10(b). Although the reasonable results were obtained, this method for finding optimum process condition was very intuitive. Hence GA was selected and used as an optimization method. The flow chart of this numerical procedure was represented in Fig. 11.

In case of 3-step sequential injection process, the GA search space was considered to the gate locations at second

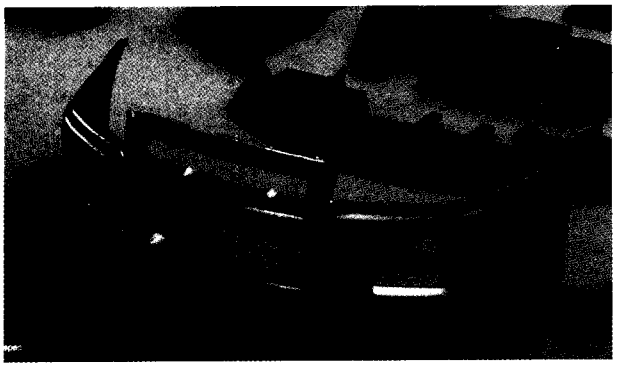

(a)

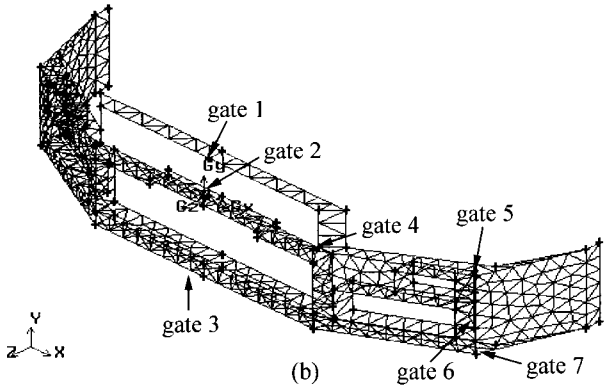

(b)

Fig. 9. 3-dimensional complex structure of the automobile bumper core.
(a) photograph
(b) finite element mesh and gate locations

Table 3. Processing conditions and fill times in complex structure

Injection Type	Case No.	Gate Loation	Fill Time(sec)
Simultaneous Injection	1	2	3570
	2	4	1145
	3	4,6	534
	4	1,2,3	1673
Sequential Multi-gate (2step)	5	1,2,3→4	1059
	6	1,2,3→5	1132
	7	1,2,3→6	1112
	8	1,2,3→7	1058
Sequential Injection (3step)	9	1,2,3→4→5	782
	10	1,2,3→4→6	762
	11	1,2,3→4→7	893

and third steps because gate locations at first step was fixed. The pressure was set up to 60 *psi* at every gate. Therefore the two parameters were discretized and then translated into a binary string of length 18. The nominal GA of this study used binary coding, initial random selection, single-point crossover, jump and creep mutation, elitism and one child per parents. The population size

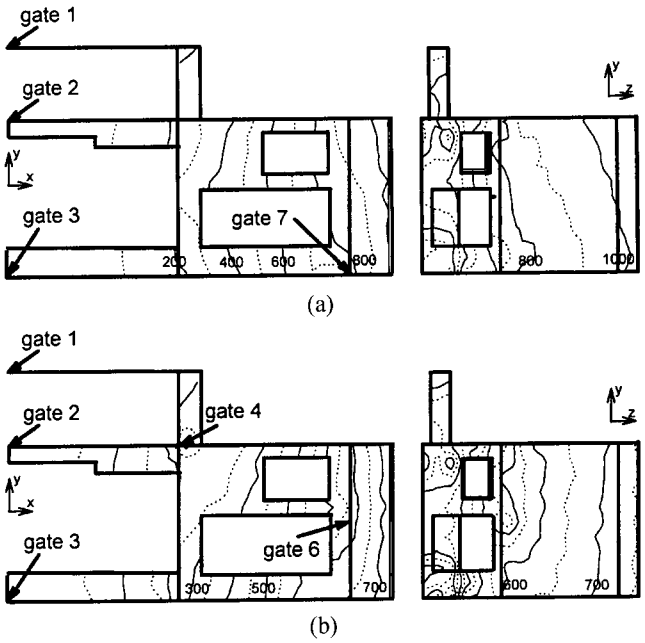

Fig. 10. Numerical flow front locations in the filling of complex structure.
(a) case 8 in Table 3 : $t_{fill,sim}$ = 1058 sec
(b) case 10 in Table 3 : $t_{fill,sim}$ = 762 sec

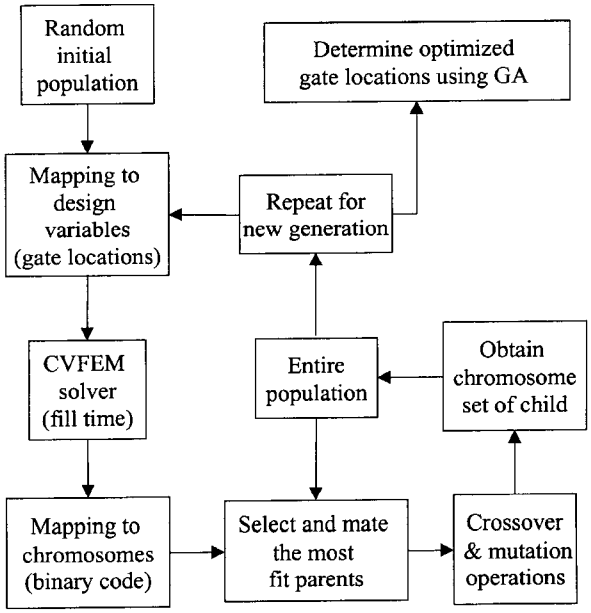

Fig. 11. Flow diagram of optimization process by using GA.

n_{pop} was set to 10, 25 and 100, the probability of crossover p_{cross} to 0.5, the jump mutation probability p_{jump} to $1/n_{pop}$ and the creep mutation probability p_{creep} to $2/n_{pop}$, respectively. As shown in Fig. 12, the optimum value was obtained at generation number 15 in case of population number 25. The optimum gate locations were determined to the node number 82 at second step and the node number 135 at third step. The final gate locations and their flow patterns were

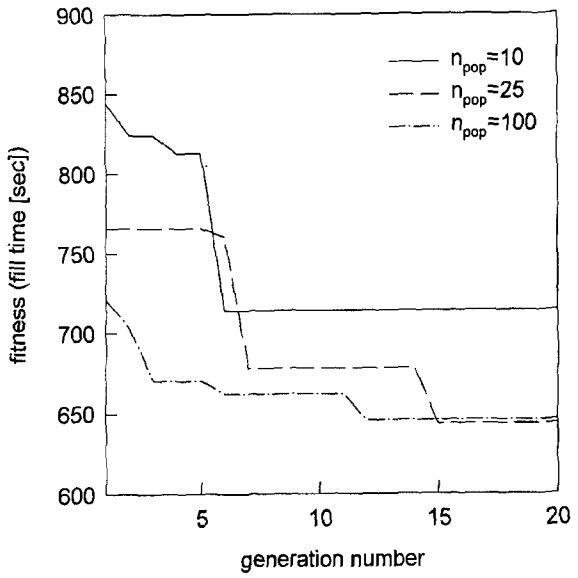

Fig. 12. Fitness (fill time) with generation number in GA.

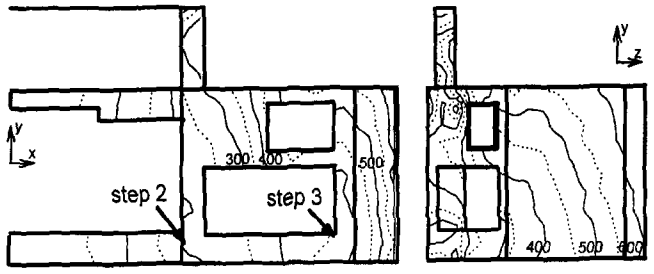

Fig. 13. Optimized gate locations and calculated flow fronts in the filling of complex structure. ($t_{fill,sim}$ = 644 sec).

represented in Fig. 13. When the optimized fill time by GA was compared with that by intuitive method, the former result was more reduced about 100 seconds than the latter one.

5. Conclusions

In this study, numerical program was developed for isothermal mold filling in the RTM process by CVFEM and its visualization experiments were carried out. The results of numerical simulation showed a good correspondence with that of the experimental. We compared the various processing schemes, these were single, sequential, and simultaneous injection techniques. The sequential injection scheme was confirmed to be very useful technique since it reduced the fill time without an increase void content and injection pressure.

In order to compare fill time by optimization process with that by determined intuitively, the complex automobile bumper core was chosen as a target model. For sequential 3-step injection process, we determined the gate location using the GA which could reduced the fill time more than 100 sec. This developed CVFEM, coupled interactively with GA, was used as an effective searching technique for determining optimum gate locations in order to minimize fill time in complex geometry.

6. Nomenclature

F : fill factor
G : dimensionless penetration length
h : height
$\bar{k}$: permeability tensor
n : number of fiber mat
P : pressure
t : thickness of the mold cavity
$\bar{v}$: average velocity
$\underset{v}{\rho}$: velocity vector

Greek Letters

δ_f : dimensionless radial extent ($= R_f/R_o$)
ϕ : porosity
Φ : dimensionless flow time
Γ : surface integration
μ : viscosity
ρ : density
Ω : line integration
ξ : surface density

References

Bruschke, M. V. and S. G. Advani, 1990, A finite element/control volume approach to mold filling in anisotropic porous media, *Polym. Compos.* **11**, 398.

Caroll, L., 1996, Chemical laser modeling with genetic algorithms, *Preprint of AIAA Journal.* **34**, 338.

Caroll, L., 1996, Genetic algorithms and optimizing chemical oxygen-iodine lasers, *Developments in Theoretical and Applied Mechanics.* **18**, 411.

Catoen, P., 1993, Designing and selecting quality hot-runner systems, *Plast. Eng.*, Apr. 45.

Chan, A. W. and R. J. Morgan, 1992, Sequential multiple port injection for resin transfer molding of polymer composites, *SAMPE Quartery*, Oct.

Chan, A. W. and S. T. Hwang, 1988, Mold-filling simulations for the injection molding of continuous fiber-reinfored polymer, *Polym. Eng. Sci.* **28**, 333.

Goldberg, E., 1989, Genetic Algorithms in Search, Optimization & Machine Learning, Addison-Wesley Publishing Co., Massachusetts.

Mathur, R., B. K. Fink and S. G. Advani, 1999, Use of genetic algorithms to optimize gate and vent locations for the resin transfer molding process, *Polym. Compos.* **20**, 167.

Noller, R., 1991, Tight-tolerance design, *Plast. Eng.*, May., 23.

Pandelidis, I. and Q. Zou, 1990, Optimization of injection molding design. Part I: gate location optimization, *Polym. Eng. Sci.*

30, 873.

Pandelidis, I. and Q. Zou, 1990, Optimization of injection molding design. Part II: molding conditions optimization, *Polym. Eng. Sci.* **30**, 883.

Phelan Jr., F. R., 1997, Simulation of the injection process in resin transfer molding, *Polym. Compos.* **18**, 460.

Shin, K. H., H. S. Ryu, and J. W. Lee, 1998, Use of resin position sensor to monitor viscosity during cure, *Theories and Applications of Rheology.* **2**, 241

Wu, C. J. and L. W. Hourng, 1995, Permeable boundary condition for numerical simulation in resin transfer molding, *Polym. Eng. Sci.* **35**, 1272.

Yoo, Y. E. and W. I. Lee, 1996, Numerical simulation of the resin transfer mold filling process using the boundary element method, *Polym. Comp.* **17**, 368.

Young, W. B., K. Han, L. H. Fong, L. J. Lee and M. J. Liou, 1991, Flow simulation in molds with preplaced fiber mats, *Polym. Compos.* **12**, 391.